Intestinal LKB1 loss drives a pre-malignant program along the serrated cancer pathway

Plugge S.F.[#,1], Ma H.[#,1,2], van der Vaart J.Y. [#,1], Sprangers J.[1], Morsink F.H.M.[2], Xanthakis D.[1], Jamieson C.[1], Keijzer A.R.[1], Margaritis T[3]., Candelli T.[3], Straver R.[1], de Ridder J.[1], Holstege F.C.P.[3, 4], de Leng W.W.J.[2], Offerhaus G.J.A.[2], Merenda A.*[,1], Maurice M.M.*,[1]

1. Center for Molecular Medicine and Oncode Institute, University Medical Center Utrecht, Utrecht, The Netherlands
2. Department of Pathology, University Medical Center Utrecht, Utrecht, The Netherlands
3. Princess Maxima Center for Pediatric Oncology, Utrecht, Utrecht, The Netherlands
4. Center for Molecular Medicine, University Medical Center Utrecht, Utrecht, The Netherlands

[#]These authors contributed equally

*Corresponding authors (a.merenda@huborganoids.nl & m.m.maurice@umcutrecht.nl)

Grant support

This work is part of the Oncode Institute, which is partly financed by the Dutch Cancer Society. This work was supported by the China Scholarship Council (to H.M.), the Dutch Cancer Society KWF Grant 13112 (to M.M.M.), Zon-MW TOP grant 91218050 (to M.M.M.) and the Netherlands Organization for Scientific Research (NWO) Gravitation programme IMAGINE! (project number 24.005.009) (to M.M.M.).

Conflict of interest

M.M.M. is co-founder and shareholder of Laigo Bio and inventor on patents related to membrane protein degradation; J.R. is co-founder of Cyclomics BV., a genomics company. All other authors declare to have no conflict of interest.

Data availability

The scRNA-seq and bulk RNA-seq data generated in this study will be uploaded to Gene Expression Omnibus (GEO) upon publication. If needed prior publication, data can be requested via the corresponding author.

Author contributions

S.F.P, H.M., J.Y.V., A.M. and M.M.M., conceived and designed the experiments. S.F.P, H.M., J.Y.V., A.M., D.X., F.H.M.M., C.J. and A.R.K performed the experiments. S.F.P, H.M., A.M., J.Y.V., J.S., T.M., T.C., R.S., J.R., F.C.P.H., G.J.A.O. and M.M.M. analyzed the data. W.W.J.L. and G.J.A.O. provided patient material. S.F.P, H.M., A.M., J.Y.V. and M.M.M. wrote the manuscript, which was reviewed by all authors.

Acknowledgements

The authors thank members of the Maurice laboratory for helpful discussions and suggestions. PiggyBac Transposase and pPB-CAG-rtTA_Hygromycin were a kind gift from B.K. Koo.

Abstract

Background & Aims

Heterozygous inactivating mutations of Liver Kinase B1 (LKB1) are causative to the Peutz-Jeghers syndrome (PJS), a hereditary disease characterized by gastrointestinal polyposis and increased cancer susceptibility. While LKB1 loss-induced polyp formation has been ascribed to non-epithelial tissues, how LKB1 deficiency increases cancer risk of patients by altering the phenotypical landscape and hierarchical organization of epithelial tissues remains poorly understood.

Methods

Using CRISPR/Cas9, we generated heterozygous and homozygous Lkb1-deficient mouse small intestinal organoids. These organoids were characterized by a combined approach that integrates imaging, bulk and single-cell RNA sequencing and growth assays. Our findings were validated in human PJS-derived tissues using immunohistochemistry and linked to colorectal cancer profiles using the TCGA cancer database.

Results

Our results reveal that heterozygous Lkb1 loss is sufficient to push cells into a premalignant transcriptional program associated with serrated colorectal cancer, which is further amplified by loss-of-heterozygosity. This altered epithelial growth state associates with persistent features of regeneration and enhanced EGFR ligand and receptor expression, conferring niche-independent growth properties to Lkb1-deficient organoids. Moreover, LKB1 loss-of-function mutations co-occur with serrated colorectal cancer driver mutations for which synergistic cooperation was experimentally confirmed for Kras mutation and Lkb1-deficiency by assessing growth properties and transcriptomes.

Conclusions

Heterozygous loss of LKB1 pushes intestinal cells into a chronic regenerative state which is amplified upon loss-of-heterozygosity. Lkb1-deficiency thereby establishes fertile ground for serrated colorectal cancer formation in the intestine, explaining the increased cancer risk observed in PJS.

Keywords: Peutz-Jeghers Syndrome; Serrated tumors; Colorectal cancer; Organoids; Regeneration

Introduction

Peutz-Jeghers syndrome (PJS) is a hereditary genetic disorder affecting approximately 1:50.000-1:200.000 individuals worldwide[1]. PJS is characterized by the formation of benign hamartomatous polyps throughout the gastrointestinal (GI) tract, which necessitates periodical surgical resection. Additionally, patients carry an increased risk of developing early-onset epithelial tumors, particularly within the GI tract (up to 66%), breast (up to 54%), pancreas (up to 36%) and gonads[1–3], resulting in a cumulative lifetime risk of 93%[3]. Moreover, PJS patients are predisposed to small intestinal cancers that rarely develop in the general population (0.03% compared to 13% in PJS)[2,4].

PJS is caused by heterozygous inactivating mutations in the tumor suppressor gene Liver Kinase B1 (*LKB1/STK11*)[5,6]. Of note, inactivation of *LKB1* is also linked to the formation of sporadic cancers such as lung carcinoma, melanoma, pancreatic and cervical cancers[7,8]. The *LKB1* gene encodes for a serine/threonine kinase involved in diverse cellular processes, including energy metabolism, cell adhesion, DNA methylation and apicobasal polarity[9–11]. Loss of heterozygosity (LOH) of *LKB1* is a driving force of cancer development, since LOH occurs in over 64% of PJS-derived carcinomas[12,13].

Recent studies using murine models revealed that *Lkb1* loss in non-epithelial lineages suffices to induce the development of GI polyps resembling those observed in PJS patients[14–17]. This led to a reevaluation of *Lkb1*'s role in non-epithelial tissues, with an emphasis on polyposis formation. The relationship between polyp formation and cancer predisposition in PJS patients however remains highly debated, as LOH and dysplastic transformation of PJS polyps appear to be very rare compared to other polyposis syndromes like familial adenomatous polyposis (FAP)[12,13,18,19].

Since *LKB1* loss mediates predisposition to carcinoma development in multiple epithelial tissues irrespective of polyp formation, we hypothesize that epithelial-intrinsic alterations may sensitize these tissues to malignant transformation. Notably, LKB1 deficiency in the intestinal epithelium itself does not mediate polyp formation but was shown to alter secretory cell fate specification[14,20–22]. Despite these advancements, how alterations in intestinal epithelial organization due to *LKB1* predispose for cancer development in PJS patients remains poorly understood.

Here, we model *mono*- and *bi*-allelic inactivation of *Lkb1* in small intestinal organoids to investigate how *Lkb1* loss affects the intestinal epithelial cellular and transcriptional landscape. We uncover that *Lkb1* loss promotes features of epithelial transformation linked to the serrated pathway for intestinal carcinogenesis. These features include loss of classical adult stem cell populations, activation of regeneration-related transcriptional programs, intestinal-to-gastric cellular transdifferentation, and the acquirement of niche-independent growth properties. Our findings argue that *Lkb1* loss mediates epithelium-wide activation of a pre-cancer program, providing an explanation for the increased cancer risk observed in PJS patients. By linking *Lkb1* loss to a major pathway for colorectal cancer (CRC) development, these findings pave a path for the development of new strategies for prevention, surveillance and precision treatment of PJS tumors as well as other malignancies harboring *LKB1*-inactivating mutations.

Materials and Methods

Organoid culture

Small intestinal mouse organoids were established from crypts isolated from the small intestine of wild-type mice, as previously described[23]. Organoids were grown in Matrigel (Corning) or BME (Cultrex) and passaged every 6-8 days as previously described[23]; their medium was refreshed every 2-3 days. For medium composition see supplementary materials.

Organoid electroporation

For generation of mutant and overexpression organoids, mouse organoids were expanded in ENR medium without antibiotics and supplemented with 50% Wnt3a-conditioned medium (homemade) and 1mM Nicotinamide (Sigma-Aldrich). Electroporation of organoids was performed as previously described using a NEPA21 (NEPAGENE) electroporator[24]. After selection, single organoids were manually picked for clonal expansion and then genotyped. For plasmids and organoid selection see supplementary materials. Genomic DNA was isolated using the DNA micro kit (Qiagen) according to the manufacturer's instructions and PCR amplification was performed using the GoTaq Flexi DNA polymerase kit (Promega). Organoid genotype was confirmed by Sanger sequencing. Primers are listed in supplementary materials**.**

Immunofluorescence

Organoids were seeded in 15-well Ibidi chambers after passaging and fixed 3-4 days later in 4% Paraformaldehyde (Sigma-Aldrich). After fixation organoids were washed with cold PBS and permeabilized with PBD0.2T and incubated with primary antibodies diluted in PBD0.2T buffer at 4°C overnight. Washes were performed with PBD0.2T buffer and secondary antibodies were incubated 2-3 hours at room temperature. All antibodies are described in supplementary materials. Images were acquired with a Zeiss LSM700 or LSM880 confocal microscope.

Patient tissue samples

Patient material was collected from the pathology archives of Dutch hospitals. Tissues of five PJS patients were included in this study. Five normal controls were randomly selected.

Immunohistochemistry

Fresh mouse small intestinal organoids were fixed in 4% formaldehyde three days after splitting for 1 hour followed by dehydration in 25%, 50% and 70% ethanol and embedding in paraffin. 4µm FFPE organoid or PJS patient tissue sections were obtained, deparaffinized, blocked in 0.3% H2O2 in methanol for 20 minutes. Antigen retrieval was performed in Tris/EDTA buffer (10 mM/1 mM; pH 9.0) or sodium-citrate buffer (0,01 M/pH6.0) for 20 minutes at 100°C. Nonspecific binding sites were blocked using Protein Block Serum-free (DAKO) for 10 minutes, followed by primary antibody incubation. Antibody binding was visualized using the using BrightVision Goat-anti-Rabbit/Poly-AP and BrightVision Goat-anti-Mouse/Poly-HRP (VWR/ImmunoLogic), with DAB as chromogen (Sigma-Aldrich). Sections were counterstained with Haematoxylin or neutral red and mounted using Pertex. Primary antibodies are described in supplementary materials.

Bulk RNA sequencing

Organoids were lysed in RLT lysis buffer (Qiagen) 3-5 days after passaging. Biological triplicates were employed. RNA was obtained using the Qiagen QiaSymphony SP (Qiagen) according to the manufacturer's protocol. For data analysis see supplementary materials.

Single cell RNA sequencing

Single cells from organoid were harvested using TrypLE incubation at 37 °C, four days after passaging. Cells were filtered through a 40 µm nylon cell strainer (Falcon). scRNA-seq was performed according to the Sort-seq protocol[25]. Libraries were sequenced on an Illumina NextSeq500 at paired-end 60- and 26-bp read length and 75,000 reads per cell. For data analysis see supplementary materials.

Results

Lkb1 bi-allelic loss results in phenotypic heterogeneity and increased self-renewal potential of small intestinal organoids.

To study the role of *Lkb1* loss in the intestinal epithelium, we employed CRISPR/Cas9 technology to generate *Lkb1*-deficient mouse small intestinal organoid lines. Targeted organoids were cultured transiently in WENR (see supplementary material) to enhance outgrowth efficiency[26]. In these conditions, organoids acquire a cystic morphology, due to the expansion of stem cells[23,27]. To obtain genotypically clonal organoid cultures that are heterozygous or homozygous for *Lkb1* loss, organoids were grown from single cells. Subsequently, cultures were transferred to ENR medium, allowing for cellular differentiation and formation of typical budding structures resembling the *in vivo* crypt-villus axis[23]. Clones that transitioned into budding organoids over 4 passages were identified as either wild-type (WT), heterozygous (*Lkb1*$^{+/-}$) or homozygous knockout for *Lkb1* (*Lkb1*$^{bud\ -/-}$) (Figure 1A-C). Notably, budding *Lkb1*$^{-/-}$ organoid cultures displayed remnants of dead cells at their basal side (Figure 1C), validated by cleaved caspase-3 staining (Figure 1D). By contrast, in WT and *Lkb1*$^{+/-}$ organoids dying cells were extruded from the apical side and shed into the lumen, in line with earlier reports (Figure 1D)[23]. Mislocalization of dead cells in *Lkb1*$^{bud\ -/-}$ organoid cultures was corrected by wild-type LKB1 overexpression in these organoids, indicating this is a consequence of Lkb1 loss (Figure S1B-C).

A fraction of targeted organoid clones failed to revert into budding structures in ENR medium (Figure S1A). These persistent cystic clones exhibited homozygous loss of *Lkb1* (*Lkb1*$^{cys\ -/-}$). Thus, homozygous Lkb1 loss manifested in two distinct morphologies, budding and cystic. Reversal of cystic morphology of *Lkb1*$^{cys\ -/-}$ organoids by reintroduction of LKB1 expression was not possible, as LKB1^{+}/mCherry^{+} cells were rapidly lost over time in these organoids (Figure S1B, D), potentially due to competition by Lkb1$^{cys\ -/-}$ cells[28]. Next, we examined whether *Lkb1* loss alters the ability of intestinal organoids to reconstitute organoids from single cells, as a proxy for their self-renewal capacity. While WT and budding *Lkb1*-deficient organoids displayed similar outgrowth rates, cystic *Lkb1*$^{cys\ -/-}$ organoids carried a significantly improved capacity to form organoids upon seeding of single cells (Figure 1E).

To rule out that the observed phenotypes are caused by unintended gRNA-induced mutations rather than *Lkb1* loss, we employed an alternative, non-overlapping *Lkb1*-targeting gRNA (gRNA2). Targeting *Lkb1* with gRNA2 led to similar morphologic changes, including shedding of dead cells at the basal side and a divergent budding and cystic morphology for homozygous *Lkb1* loss (Figure S2). Moreover, newly generated *Lkb1*$^{cys\ -/-}$ clones also displayed superior reconstitution potential compared to their homozygous budding counterparts (Figure S2C). We conclude that *Lkb1*-deficiency results in specific organoid phenotypes related to loss of one or both alleles of *Lkb1*.

Lkb1 loss alters the number, morphology and positioning of secretory cells.

To investigate whether our *Lkb1*-mutant organoid lines serve as representative models for intestinal epithelial *Lkb1* loss *in vivo*, we examined alterations in localization and morphology of Paneth (Lyz^{+}) and goblet (Muc2^{+}) cells previously reported for the *Lkb1*-mutant mouse intestine[20,21]. Compared to WT organoids, Lyz1^{+} cells in *Lkb1*$^{+/-}$ and *Lkb1*$^{bud\ -/-}$ organoids were scattered beyond the crypt region into the villus domain (Figure 2A, Figure S3A). Additionally, in both WT and *Lkb1*$^{+/-}$ organoids, Muc2^{+} cells were

sparse and located to the villus region, while *Lkb1*$^{bud\ -/-}$ organoids displayed increased Muc2^{+} cells that were found scattered throughout the crypt-villus axis (Figure 2B). These observations resemble reported aberrancies in Paneth and goblet cell numbers and localization in *Lkb1*-deficient mouse intestine *in vivo*[20]. Conversely, *Lkb1*$^{cys\ -/-}$ organoids lacked Lyz1^{+} cells but did form Muc2^{+} cells that are usually lacking in cystic organoids[29], indicating that secretory lineage specification is also altered within these organoids (Figure 2A-B).

We next compared these findings to the intestinal tissue of human PJS patients. The number and location of MUC2^{+} cells per intestinal crypt were similar in healthy donors and PJS patients (Figure 2C, Figure S2B-C). However, compared to healthy donors, LYZ1^{+} cells were mislocalized within the PJS mucosa (Figure 2D, Figure S3D-E). Thus, heterozygous loss of *LKB1* in PJS patient-derived intestines leads to mislocalization of LYZ1^{+}cells without altering MUC2^{+} cell distribution, similar to our observations in *Lkb1*$^{+/-}$ organoids.

To examine *Lkb1* loss-induced alterations in secretory cell morphology at the ultrastructural level, we employed electron microscopy. In WT intestinal organoids, Paneth cells displayed a typical apical accumulation of spherically-shaped secretory granules filled with electron-dense content (Figure 2E)[23,30], while *Lkb1*$^{+/-}$ Paneth cells carried granules with an abnormal 'sausage-shaped' electron-dense core (Figure 2E). In *Lkb1*$^{bud-/-}$ Paneth cells, granules displayed a small electron-dense core surrounded by a peripheral electron-lucent halo (Figure 2E). WT goblet cells were columnar-shaped and contained typical large translucent mucus-filled granules (Figure 2F)[31,32]. *Lkb1*$^{+/-}$ mucus-secreting cells however were rounded and flattened while *Lkb1*$^{bud\ -/-}$ goblet-like cells display granules with an unusual electron-dense core (Figure 2F). In addition, in *Lkb1*$^{cys-/-}$ organoids the mucus-like granule content was frequently lost during EM preparation, suggesting an altered mucin composition and explaining the limited number of observed Muc2^{+} cells (Figure 2F). Morphologically, Paneth- and goblet-like cells in *Lkb1*-deficient organoids looked like 'intermediate' cells that were proposed previously to represent transition states between undifferentiated and mature cells[31], suggesting that *Lkb1* loss may interfere with terminal differentiation of secretory cells. Furthermore, although previous studies[53] identified roles of *LKB1* in apical brush border formation using 2D human cell lines, our EM images showed no obvious defects in brush border formation in *Lkb1*-deficient organoids (Figure S3F).

Our findings thus reveal that *Lkb1* loss in budding organoids induces alterations in secretory cell number, localization and morphology similar to *in vivo* mouse models and PJS patient intestines, thus validating these organoids as tools for modelling epithelial alterations in PJS. While *Lkb1*$^{cys\ -/-}$ organoids are more difficult to directly link to PJS epithelial organization *in vivo*, they may represent an intermediate state (acquired via LOH) in cancer progression. We therefore included all clonal organoid variants for further characterization.

***Lkb1* mono- and bi-allelic loss induces incremental expression of a regenerative gene signature.**

To examine how *Lkb1* loss affects the epithelial landscape, we determined transcriptional changes using bulk mRNA sequencing. Compared to WT organoids, we observed differential expression of 1298, 2312 and 7816 genes in *Lkb1*$^{+/-}$, *Lkb1*$^{bud\ -/-}$ and *Lkb1*$^{cys\ -/-}$ organoids, respectively (Supplementary Table 1).

Using gene set enrichment analysis (GSEA) we examined the consequences of *Lkb1*-loss on transcriptional gene profiles representing individual intestinal cell types[33]. All *Lkb1*-deficient clones showed significant downregulation of gene sets linked to mature Paneth cells, whereas goblet cell gene sets were

enriched within *Lkb1*$^{bud\ -/-}$ organoids in comparison to WT organoids, again suggesting alterations in secretory cell lineage specification (Figure 3A). Noticeably, the *Lgr5*$^{+}$ adult stem cell signature[33] was downregulated in all *Lkb1*-deficient clones (Figure 3A, Figure S4A), reminiscent of the growth state of fetal intestinal spheroids reliant on *Lgr5*-negative progenitors[34]. Indeed, we uncovered a gradual enrichment of an embryonic spheroid gene signature in *Lkb1*-deficient organoids[34], correlating with the number of lost *Lkb1* alleles in the budding phenotypes (Figure 3A-B). This transition was further enhanced in *Lkb1*$^{cys\ -/-}$ versus *Lkb1*$^{bud\ -/-}$ organoids (Figure S4B). Previous studies linked a transient upregulation of a fetal-like intestinal gene signature to epithelial remodeling and collagen deposition during injury repair[35–39]. In line, *Lkb1*-deficient organoid clones also exhibited enrichment of gene signatures associated with intestinal regeneration following damage or infection (Figure 3A, Figure S4A).

To confirm that *Lkb1*-deficiency rather than organoid morphology mediates activation of a regenerative program in Lkb1$^{cys\ -/-}$ organoids, we analyzed the transcriptomes of *Apc*$^{-/-}$ and Wnt-treated cystic organoids that are WT for *Lkb1*[27]. *Lkb1*$^{cys\ -/-}$ organoids were significantly enriched for expression of regenerative gene sets compared to *Apc*$^{-/-}$ and Wnt-treated organoids (Figure S4C). These findings confirm that *Lkb1* loss itself promotes a regenerative state, although morphology may contribute to the enhancement of this phenotype.

Furthermore, *Lkb1*-deficient clones, and control fetal intestinal organoids (E16.5), displayed increased expression of the fetal marker Anxa1[35], which was absent in WT adult intestinal organoids (Figure 3C, Figure S4D). Additionally, a dysplastic region of PJS patient-derived duodenum was marked with ANXA1-positive epithelial cells, while non-transformed PJS and healthy donor duodenum epithelium remained negative (Figure 3D). These findings indicate that *Lkb1*-deficiency converts the epithelium into a primed regenerative state that is already apparent upon monoallelic *Lkb1* loss, which mirrors the PJS intestinal epithelium.

Lkb1-deficient organoids show a Yap-induced regenerative state and display intra-epithelial self-sufficiency for Egf.

Over recent years, Yap signaling was placed central to intestinal regeneration[40]. Additionally, *LKB1* was identified as a negatively regulator of the Hippo-Yap pathway[41]. We therefore wondered if *Lkb1* loss may activate Yap signaling in intestinal epithelial organoids. Indeed, we identified enhanced expression of multiple Yap-regulated gene signatures[40,42] in *Lkb1*-deficient organoids (Figure 4A, Figure S5A). These signatures contain key YAP target genes including *Ctgf*, *Amotl1* and *Cyr61*[42]. Notably, Yap target gene expression increased with the number of lost *Lkb1* alleles (normalized enrichment scores of 2.01 and 2.68, respectively). Yap target gene expression was further enhanced in *Lkb1*$^{cys\ -/-}$ organoids compared to their budding counterparts, consistent with their enhanced regenerative transcriptional program (Figure S5A). Immunofluorescence staining confirmed increased Yap protein expression and nuclear localization in both budding and cystic *Lkb1*$^{-/-}$ organoids (Figure 4B-C, Figure S5B-C).

YAP pathway activation is well-known to enhance EGF family ligand expression during regeneration[40,43–45]. In line, *Lkb1*-deficient organoids showed upregulated expression of Egf ligands and receptor family members, correlating with *Lkb1* allelic loss and alterations in organoid morphology (Figure 4-ED, Figure S5D-E). Given the dependency of healthy intestinal organoids on Egf, we examined if *Lkb1*-deficient organoids may grow without Egf. Unlike WT organoids, all *Lkb1*-deficient organoids grew out

without Egf supplementation (Figure 4F-G, Figure S5F-G). To ensure this was due to endogenous ligand secretion and not downstream pathway activation, we treated the organoids with Gefitinib, an EGFR inhibitor. All organoid lines remained sensitive to EGFR inhibition (Figure 4H, Figure S5H), confirming endogenous EGF production as the driver.

These results demonstrate that *Lkb1* loss induces a Yap-induced regenerative state and EGF ligand self-sufficiency. As niche-independent growth is a hallmark of cancer progression[46], these results suggest that *Lkb1*-deficient epithelial cells carry a growth advantage which may promote tumorigenesis initiation.

Lkb1-deficiency mediates reprogramming of intestinal stem cells into a regenerative state.

To analyze how *Lkb1* loss alters intestinal lineage specification and cellular hierarchies, we subjected WT and *Lkb1*-deficient organoids to single cell RNA sequencing. We included an analysis of mouse fetal intestinal organoids, to explore a potential overlap with fetal gene expression. Unsupervised clustering identified 19 distinct clusters (Figure S6A). $Lkb1^{cys\ -/-}$ organoids and fetal cells clearly separated, while $Lkb1^{bud\ -/-}$ and $Lkb1^{+/-}$ organoids more closely resembled WT cells (Figure 5A). These findings thus indicate that although $Lkb1^{cys\ -/-}$ organoids express a fetal-like gene program they do not fully convert into a fetal state (Figure 5A). Furthermore, $Lkb1^{cys\ -/-}$ organoids harbor a homogenous cell population distinct from all budding organoid clusters, lacking a known intestinal cellular identity. We therefore annotated cell types only in budding organoid lines, using intestinal cell type gene signatures (Figure 5B, Figure S6B-I)[33]. As the gene signatures for Paneth and goblet cells mapped to the same cluster (Figure S6E, S6H), we marked this cluster as secretory progenitors, similar to previous reports[47]. We reclustered all cells from the budding organoids (WT, $Lkb1^{+/-}$ and $Lkb1^{bud\ -/-}$) for further analyses (Figure 5C-D). Cell type fraction analysis revealed an increased fraction of secretory progenitor cells in $Lkb1^{bud\ -/-}$ organoids (Figure 5E), confirming alterations in secretory cell differentiation. This increase corresponded with a decrease in enterocyte numbers, suggesting a shift in differentiation from absorptive towards secretory lineages (Figure 5E). Furthermore, we identified 'intermediate' cells in *Lkb1*-deficient organoids that co-express features of Paneth and goblet cells (Figure 5F), in line with our ultrastructural morphological analysis.

Notably, *Anxa1* expression in $Lkb1^{bud\ -/-}$ organoids was mainly enhanced within stem and transit amplifying (stem/TA) cell clusters, indicating that these progenitor populations drive the epithelium's regenerative state (Figure 5G). Reclustering of stem/TA cell populations showed distinct clusters for WT, $Lkb1^{+/-}$ and $Lkb1^{bud\ -/-}$ stem/TA cells (Figure S6J-K). GSEA on genes differentially expressed between WT stem cells and *Lkb1*-deficient stem cells (Supplementary Table 2) revealed enrichment of goblet cell gene expression within *Lkb1*-deficient stem cell populations (Figure 5H-I). Furthermore, *Lkb1*-deficient stem cells displayed enrichment of regenerative and Yap gene signatures, depletion of the $Lgr5^{+}$ stem cell signature, and increased expression of Anxa1 (Figure 5H, J). These findings support a model in which *Lkb1* loss induces a regenerative response originating from the stem cell compartment of the intestinal epithelium.

In conclusion, our results argue that *Lkb1*-deficient stem/TA cells reside in a regenerative state and preferentially differentiate towards secretory cell lineages.

Lkb1 loss drives a pre-malignant program along the serrated pathway which is amplified by additional _Kras_ mutations.

Next, we aimed to obtain insight in how transcriptional reprogramming induced by *Lkb1* loss may promote cancer predisposition. CRC mainly develops via two pathways: the classical adenoma-carcinoma sequence, initiated by bi-allelic *APC* mutations, and the serrated cancer pathway, initiated by *BRAF* or *KRAS* mutations[48,49]. We examined expression of gene sets linked to these CRC routes to assess if *Lkb1* loss drives entry into one of these pathways. All *Lkb1*-deficient organoids display significant enrichment of genes that were previously found to mark neoplastic populations of serrated-specific cells (SSC[34], iCMS3[36]), which increased with the number of lost *Lkb1* alleles (normalized enrichment scores of 1.70 and 2.16, respectively) (Figure 6A, Figure S7A). Single cell analysis confirmed this trend, attributing the increase of the serrated gene program to *Lkb1*-deficient stem cell populations (Figure S8). This increase was accompanied by the loss of adenoma-specific genes (Figure 6A, Figure S7A, ASC[34], iCMS2[36]). and upregulation of expression of common gastric markers like *Aqp5*, *Tacstd2* [*Trop2*], *Tff2*, and *Msln* (Figure 6A-B, Figure S7A-B, Supplementary Table 1), indicating the occurrence of intestinal-to-gastric cellular transdifferentiation[48].

To investigate if an *Lkb1*-deficient epithelial state is susceptible to common driver mutations in CRC, we introduced *Apc* (Figure S7C) or *Kras* mutations (Figure S7D) in *Lkb1*-deficient organoids. *Kras* mutations synergistically enhanced *Lkb1*$^{-/-}$ organoid formation from single cells, while *Apc* mutations did not (Figure 6C-D, Figure S7E-F). Bulk mRNA sequencing of double-mutant organoids showed that Lkb1 loss acts synergistically with KrasG12D mutations to drive a stepwise SSC transcriptomic shift correlated with allelic loss (Supplementary Table 3, Figure 6E, Figure S7G). By contrast, no synergism of *Lkb1* loss with ASC signature expression or with *Apc*$^{-/-}$ mutations was observed (Figure 6F, Figure S7H).

To assess whether sporadic LKB1-mutant tumors also link to the serrated pathway of CRC development, we examined The Cancer Genome Atlas (TCGA) CRC database. Indeed, we found that *LKB1*-mutant tumors are enriched for mutations associated with serrated cancers, including *BRAF*, *RNF43* and *PIK3CA*, while *APC* mutations were enriched in *LKB1* WT tumors (Figure 6G)[50,51]. *TP53* mutations were similar between groups, and *KRAS* mutations were not significantly different (Figure 6G), likely due to their occurrence in late-stage classical adenocarcinomas[49]. *LKB1*-mutant tumors also had microsatellite instable (MSI) frequency, a common trait of serrated cancers (Figure 6H)[64]. Expression of the *Lkb1*-deficient gene signature correlated with mucinous CRC, common in serrated adenocarcinomas (Figure 6I)[52], and was highly expressed in the serrated consensus molecular subtypes (CMS) CMS1 and CMS4 (Figure 6J)[49].

These results indicate that *Lkb1* loss drives cancer predisposition along the serrated CRC pathway. *Kras* mutations amplify the serrated state in *Lkb1*-deficient organoids. Furthermore, homozygous *Lkb1* loss allows for cystic organoid formation that achieves an advanced serrated state without additional oncogenic mutations. Thus, loss of *LKB1* primes the intestinal epithelium for progression along the serrated pathway.

Discussion

Over recent years, *Lkb1*-deficient mouse models have faithfully mimicked intestinal hamartomatous polyp formation, a hallmark of PJS disease. The combined findings suggest that loss of non-epithelial functions of *LKB1* contribute to PJS polyposis[14–17]. The relationship between *LKB1* loss-induced polyposis and epithelial cancer predisposition however remains highly debated and does not explain extra-intestinal cancer development[2,12,13,18]. Furthermore, the impact of heterozygous and homozygous *LKB1* loss on PJS epithelial tissue organization at the single cell level has not been addressed.

We employed mouse small intestinal organoids to understand how *Lkb1* loss affects epithelial cell identities and drives a pre-malignant state for CRC. By generating heterozygous and homozygous *Lkb1* knockouts, we aimed to model cancer predisposition and development in PJS patients, as over 64% of PJS-derived carcinomas present inactivation of the second gene copy[12,13]. Our findings argue that heterozygous *Lkb1* loss is sufficient to push cells into a premalignant program along the serrated CRC pathway, independent of the micro-environment. This premalignant program is amplified upon loss of the second allele, revealing that *LKB1*$^{+/-}$ PJS epithelia undergo significant alterations compared to healthy individuals and confirm that LOH is a driver of cancer formation.

Our organoid-based model validates the link between *Lkb1* loss and aberrant secretory cell specification *in vivo* in mice. We observed that *Lkb1*-deficiency mediates an increase in goblet cells and mucus formation and the generation of secretory cells with 'intermediate' features, both morphologically and transcriptionally. Supporting this, our newly generated *Lkb1*-deficient gene signature correlated with transcriptional profiles of mucinous subtypes of sporadic CRC. Similar secretory cell alterations induced by *Lkb1* loss may occur in other epithelial tissues, as mucinous carcinomas are common in PJS patients[53–55]. Although the underlying mechanism requires further investigation, these findings indicate a link between secretory cell alterations and cancer subtype progression.

Transcriptomic analysis revealed that *Lkb1* loss induces a dosage-dependent expression of a regenerative epithelial program. This tissue repair program was activated in standard culture conditions, without external damage, suggesting an inherent cellular response upon Lkb1 loss. We conclude that the *Lkb1*$^{+/-}$ epithelium partially shifts to a regenerative state, which is further amplified by loss-of-heterozygosity. We anticipate that, in PJS patients, external injury of the *LKB1*-mutant intestine may lock the epithelium into a chronic regenerative state, which may contribute increased tumor development. The regenerative state also showed increased *Egf* receptor family and ligand expression, endowing niche-independent properties, which is regarded as a hallmark of cancer[56].

Importantly, we uncovered that *Lkb1* loss predisposes the serrated CRC pathway, accompanied by common serrated features like gastric metaplasia, a regenerative gene program and classical stem cell depletion[48,49]. Furthermore, elevated expression of our newly generated *Lkb1*-deficient gene signature was found in serrated CRC subtypes CMS1 and CMS4, and *LKB1* mutations frequently co-occured with driver mutations of the serrated pathway. These findings suggest that PJS cancer pathways differ from the conventional APC-mutant adenocarcinomas in FAP[57].

Recently, a model proposed that different environmental triggers like microbial dysbiosis and subsequent MAPK pathway activation drive sessile serrated lesion formation[58,59]. While we currently do not know how external stressors (such as microbial dysbiosis) may affect tumor development in PJS patients, we observed that introduction oncogenic *Kras* in *Lkb1*-deficient organoids amplifies serrated features and

enhanced organoid-forming capacity. Furthermore, our results reveal that homozygous *Lkb1* loss induces two organoid phenotypes with either a budding or a cystic morphology accompanied by strongly induced serrated features. Together, our findings suggest that the PJS epithelium is sensitized to events that synergistically drive cells into a premalignant serrated state, such as intestinal damage or activating mutations in MAPK pathway components.

PJS patients require life-long monitoring for polyp resection and (pre)cancerous lesion screening. Our results argue for specific screening of serrated lesions, which may be overlooked due to their subtle histological features[60]. Diagnosed serrated lesions could be confirmed by various biomarkers including an increased MUC5AC expression linked to the absence of CDX2[48], or markers identified in this study like ANXA1.

Together, our study reveals that intestinal organoids are valuable models for *LKB1* mutation effects in PJS patients. Our findings further establish that induction of a premalignant sessile serrated program is a hallmark of PJS and provides an explanation for increased cancer incidence in PJS patients. The presented models may provide a starting point to uncover how additional mutations and environmental stressors interact with *LKB1* mutations and how stromal and immune components contribute to malignant growth of the PJS epithelium. Ultimately, in-depth knowledge on the pathways and processes involved in driving PJS epithelia into a pre-malignant state may help to design strategies that re-establish epithelial homeostasis and reduce the incidence of cancer development in PJS patients.

References

1. Beggs AD, Latchford AR, Vasen HFA, et al. Peutz-Jeghers syndrome: a systematic review and recommendations for management. Gut 2010;59:975–986.

2. Lier MGF Van, Wagner A, Mathus-Vliegen EMH, et al. High cancer risk in peutz-jeghers syndrome: A systematic review and surveillance recommendations. Am J Gastroenterol 2010;105:1258–1264.

3. Giardiello FM, Brensinger JD, Tersmette AC, et al. Very high risk of cancer in familial Peutz-Jeghers syndrome. Gastroenterology 2000;119:1447–1453.

4. Tomasetti C, Vogelstein B. Variation in cancer risk among tissues can be explained by the number of stem cell divisions. Science (80-) 2015;347:78–81. Available at: www.sciencemag.org/content/347/6217/75/suppl/DC1.

5. Hemminki A, Markie D, Tomlinson I, et al. A serine/threonine kinase gene defective in Peutz–Jeghers syndrome. Nat 1998 3916663 1998;391:184–187. Available at: https://www.nature.com/articles/34432.

6. Jenne DE, Reimann H, Nezu JI, et al. Peutz-Jeghers syndrome is caused by mutations in a novel serine threoninekinase. Nat Genet 1998 181 1998;18:38–43. Available at: https://www.nature.com/articles/ng0198-38.

7. Sanchez-Cespedes M. A role for LKB1 gene in human cancer beyond the Peutz-Jeghers syndrome. Oncogene 2007;26:7825–7832.

8. Giardiello FM, Trimbath JD. Peutz-Jeghers syndrome and management recommendations. Clin Gastroenterol Hepatol 2006;4:408–415.

9. Pierce SE, Granja JM, Corces MR, et al. LKB1 inactivation modulates chromatin accessibility to drive metastatic progression. Nat Cell Biol 2021;23:915–924. Available at: https://doi.org/10.1038/s41556-021-00728-4.

10. Kline ER, Shupe J, Gilbert-Ross M, et al. LKB1 Represses Focal Adhesion Kinase (FAK) Signaling via a FAK-LKB1 Complex to Regulate FAK Site Maturation and Directional Persistence. J Biol Chem 2013;288:17663. Available at: /pmc/articles/PMC3682567/.

11. Shackelford DB, Shaw RJ. The LKB1-AMPK pathway: Metabolism and growth control in tumour suppression. Nat Rev Cancer 2009;9:563–575. Available at: http://dx.doi.org/10.1038/nrc2676.

12. Entius MM, Keller JJ, Westerman AM, et al. Molecular genetic alterations in hamartomatous polyps and carcinomas of patients with Peutz-Jeghers syndrome. J Clin Pathol 2001;54:126–131.

13. Leng WWJ De, Westerman AM, Weterman MAJ, et al. Cyclooxygenase 2 expression and molecular alterations in Peutz-Jeghers hamartomas and carcinomas. Clin Cancer Res 2003;9:3065–72. Available at: http://www.ncbi.nlm.nih.gov/pubmed/12912958.

14. Cotton JL, Dang K, Hu L, et al. PTEN and LKB1 are differentially required in Gli1-expressing mesenchymal cells to suppress gastrointestinal polyposis. Cell Rep 2022;40:111125. Available at:

https://linkinghub.elsevier.com/retrieve/pii/S2211124722009317.

15. Poffenberger MC, Metcalfe-Roach A, Aguilar E, et al. LKB1 deficiency in T cells promotes the development of gastrointestinal polyposis. Science (80-) 2018;361:406–411.

16. Ollila S, Domènech-Moreno E, Laajanen K, et al. Stromal Lkb1 deficiency leads to gastrointestinal tumorigenesis involving the IL-11-JAK/STAT3 pathway. J Clin Invest 2018;128:402–414. Available at: https://pubmed.ncbi.nlm.nih.gov/29202476/.

17. Katajisto P, Vaahtomeri K, Ekman N, et al. LKB1 signaling in mesenchymal cells required for suppression of gastrointestinal polyposis. Nat Genet 2008;40:455–459. Available at: https://pubmed.ncbi.nlm.nih.gov/18311138/.

18. Korsse SE, Biermann K, Offerhaus GJA, et al. Identification of molecular alterations in gastrointestinal carcinomas and dysplastic hamartomas in Peutz-Jeghers syndrome. Carcinogenesis 2013;34:1611–1619. Available at: https://academic.oup.com/carcin/article/34/7/1611/2463105.

19. Fodde R. The APC gene in colorectal cancer. Eur J Cancer 2002;38:867–871.

20. Shorning BY, Zabkiewicz J, McCarthy A, et al. Lkb1 deficiency alters goblet and paneth cell differentiation in the small intestine. Morty RE, ed. PLoS One 2009;4:e4264. Available at: https://dx.plos.org/10.1371/journal.pone.0004264.

21. Gao Y, Yan Y, Tripathi S, et al. LKB1 Represses ATOH1 via PDK4 and Energy Metabolism and Regulates Intestinal Stem Cell Fate. Gastroenterology 2020;158:1401.

22. Kim Y, Lee S, Kim S, et al. LKB1 in Intestinal Epithelial Cells Regulates Bile Acid Metabolism by Modulating FGF15/19 Production. Cmgh 2022;13:1121–1139. Available at: https://doi.org/10.1016/j.jcmgh.2021.12.017.

23. Sato T, Vries RG, Snippert HJ, et al. Single Lgr5 stem cells build crypt-villus structures in vitro without a mesenchymal niche. Nature 2009;459:262–5. Available at: http://www.ncbi.nlm.nih.gov/pubmed/19329995.

24. Fujii M, Matano M, Nanki K, et al. Efficient genetic engineering of human intestinal organoids using electroporation. Nat Protoc 2015 1010 2015;10:1474–1485. Available at: https://www.nature.com/articles/nprot.2015.088.

25. Muraro MJ, Dharmadhikari G, Grün D, et al. A Single-Cell Transcriptome Atlas of the Human Pancreas. Cell Syst 2016;3:385. Available at: /pmc/articles/PMC5092539/.

26. Pleguezuelos-Manzano C, Puschhof J, Brink S van den, et al. Establishment and Culture of Human Intestinal Organoids Derived from Adult Stem Cells. Curr Protoc Immunol 2020;130. Available at: https://currentprotocols.onlinelibrary.wiley.com/doi/10.1002/cpim.106.

27. Merenda A, Fenderico N, Maurice MM. Wnt Signaling in 3D: Recent Advances in the Applications of Intestinal Organoids Trends in Cell Biology. Trends Cell Biol 2020;30. Available at: https://doi.org/10.1016/j.tcb.2019.10.003.

28. Krotenberg Garcia A, Fumagalli A, Le HQ, et al. Active elimination of intestinal cells drives oncogenic growth in organoids. Cell Rep 2021;36:109307. Available at: https://linkinghub.elsevier.com/retrieve/pii/S2211124721006835.

29. Sato T, Es JH Van, Snippert HJ, et al. Paneth cells constitute the niche for Lgr5 stem cells in intestinal crypts. Nature 2011;469:415–418.

30. Satoh Y, Yamano M, Matsuda M, et al. Ultrastructure of Paneth cells in the intestine of various mammals. J Electron Microsc Tech 1990;16:69–80. Available at: https://onlinelibrary.wiley.com/doi/full/10.1002/jemt.1060160109.

31. Troughton WD, Trier JS. Paneth and goblet cell renewal in mouse duodenal crypts. J Cell Biol 1969;41:251–268. Available at: http://rupress.org/jcb/article-pdf/41/1/251/1069008/251.pdf.

32. Bansil R, Turner BS. The biology of mucus: Composition, synthesis and organization. Adv Drug Deliv Rev 2018;124:3–15.

33. Haber AL, Biton M, Rogel N, et al. A single-cell survey of the small intestinal epithelium. Nature 2017;551:333–339.

34. Mustata RC, Vasile G, Fernandez-Vallone V, et al. Identification of Lgr5-Independent Spheroid-Generating Progenitors of the Mouse Fetal Intestinal Epithelium. Cell Rep 2013;5:421–432.

35. Yui S, Azzolin L, Maimets M, et al. YAP/TAZ-Dependent Reprogramming of Colonic Epithelium Links ECM Remodeling to Tissue Regeneration. Cell Stem Cell 2018;22:35-49.e7. Available at: https://doi.org/10.1016/j.stem.2017.11.001.

36. Nusse YM, Savage AK, Marangoni P, et al. Parasitic helminths induce fetal-like reversion in the intestinal stem cell niche. Nature 2018;559:109–113. Available at: http://dx.doi.org/10.1038/s41586-018-0257-1.

37. Ayyaz A, Kumar S, Sangiorgi B, et al. Single-cell transcriptomes of the regenerating intestine reveal a revival stem cell. Nature 2019;569:121–125. Available at: http://dx.doi.org/10.1038/s41586-019-1154-y.

38. Kobayashi S, Ogasawara N, Watanabe S, et al. Collagen type I-mediated mechanotransduction controls epithelial cell fate conversion during intestinal inflammation. Inflamm Regen 2022;42:49.

39. Qu M, Xiong L, Lyu Y, et al. Establishment of intestinal organoid cultures modeling injury-associated epithelial regeneration. Cell Res 2021;31:259–271. Available at: http://dx.doi.org/10.1038/s41422-020-00453-x.

40. Gregorieff A, Liu Y, Inanlou MR, et al. Yap-dependent reprogramming of Lgr5+ stem cells drives intestinal regeneration and cancer. Nature 2015;526:715–718.

41. Mohseni M, Sun J, Lau A, et al. A genetic screen identifies an LKB1-MARK signalling axis controlling the Hippo-YAP pathway. Nat Cell Biol 2014;16:108–117.

42. Pikkupeura LM, Bressan RB, Guiu J, et al. Transcriptional and epigenomic profiling identifies YAP

signaling as a key regulator of intestinal epithelium maturation. 2023. Available at: https://www.science.org.

43. Zhang J, Ji J-Y, Yu M, et al. YAP-dependent induction of amphiregulin identifies a non-cell-autonomous component of the Hippo pathway. Nat Cell Biol 2009.

44. Yang N, Morrison CD, Liu P, et al. TAZ induces growth factor-independent proliferation through activation of EGFR ligand amphiregulin. Cell Cycle 2012;11:2922–2930. Available at: https://www.tandfonline.com/action/journalInformation?journalCode=kccy20http://dx.doi.org/10.4161/cc.21386.

45. Ren F, Wang B, Yue T, et al. Hippo signaling regulates Drosophila intestine stem cell proliferation through multiple pathways. Proc Natl Acad Sci U S A 2010;107:21064–21069. Available at: https://www.pnas.org/doi/abs/10.1073/pnas.1012759107.

46. Fujii M, Shimokawa M, Date S, et al. A Colorectal Tumor Organoid Library Demonstrates Progressive Loss of Niche Factor Requirements during Tumorigenesis. Cell Stem Cell 2016;18:827–838.

47. Malagola E, Vasciaveo A, Ochiai Y, et al. Isthmus progenitor cells contribute to homeostatic cellular turnover and support regeneration following intestinal injury. Cell 2024;187:3056-3071.e17. Available at: https://linkinghub.elsevier.com/retrieve/pii/S0092867424004902.

48. Chen B, Scurrah CR, McKinley ET, et al. Differential pre-malignant programs and microenvironment chart distinct paths to malignancy in human colorectal polyps. Cell 2021;184:6262-6280.e26. Available at: https://doi.org/10.1016/j.cell.2021.11.031.

49. Aiderus A, Barker N, Tergaonkar V. Serrated colorectal cancer: preclinical models and molecular pathways. Trends in Cancer 2024;10:76–91. Available at: https://linkinghub.elsevier.com/retrieve/pii/S2405803323001954.

50. Robertson DJ, Yang VW, Crockett SD, et al. Terminology, Molecular Features, Epidemiology, and Management of Serrated Colorectal Neoplasia. Gastroenterology 2019;157:949-966.e4. Available at: http://www.gastrojournal.org/article/S0016508519411153/fulltext.

51. Day FL, Jorissen RN, Lipton L, et al. PIK3CA and PTEN gene and exon mutation-specific clinicopathologic and molecular associations in Colorectal cancer. Clin Cancer Res 2013;19:3285–3296. Available at: https://aacrjournals.org/clincancerres/article/19/12/3285/77812/PIK3CA-and-PTEN-Gene-and-Exon-Mutation-Specific.

52. Tuppurainen K, Mäkinen JM, Junttila O, et al. Morphology and microsatellite instability in sporadic serrated and non-serrated colorectal cancer. J Pathol J Pathol 2005;207:285–294.

53. Collet L, Ghurburrun E, Meyers N, et al. Kras and Lkb1 mutations synergistically induce intraductal papillary mucinous neoplasm derived from pancreatic duct cells. Gut 2020;69:704–714. Available at: https://gut.bmj.com/content/69/4/704.

54. Osoegawa A, Kometani T, Nosaki K, et al. LKB1 Mutations Frequently Detected in Mucinous Bronchioloalveolar Carcinoma. Jpn J Clin Oncol 2011;41:1132–1137. Available at:

https://academic.oup.com/jjco/article/41/9/1132/839529.

55. Sato N, Rosty C, Jansen M, et al. STK11/LKB1 Peutz-Jeghers Gene Inactivation in Intraductal Papillary-Mucinous Neoplasms of the Pancreas. Am J Pathol 2001;159:2017–2022.

56. Hanahan D, Weinberg RA. Hallmarks of Cancer: The Next Generation. Cell 2011;144:646–674.

57. Li J, Wang R, Zhou X, et al. Genomic and transcriptomic profiling of carcinogenesis in patients with familial adenomatous polyposis. Gut 2020;69:1283–1293. Available at: http://dx.doi.org/10.1136/gutjnl-2019-319438.

58. IJspeert JEG, Dekker E. Gastric metaplasia could initiate the serrated neoplasia pathway in CRC. Nat Rev Gastroenterol Hepatol 2022;19:217–218. Available at: https://doi.org/10.1038/s41575-022-00592-z.

59. Shields CED, White JR, Chung L, et al. Sensitive To Immune Checkpoint Therapy. 2022;11:1792–1807.

60. Rosty C, Hewett DG, Brown IS, et al. Serrated polyps of the large intestine: current understanding of diagnosis, pathogenesis, and clinical management. J Gastroenterol 2012 483 2012;48:287–302. Available at: https://link.springer.com/article/10.1007/s00535-012-0720-y.

61. Joanito I, Wirapati P, Zhao N, et al. Single-cell and bulk transcriptome sequencing identifies two epithelial tumor cell states and refines the consensus molecular classification of colorectal cancer. Nat Genet 2022;54:963–975. Available at: https://doi.org/10.1038/s41588-022-01100-4.

Figure legends

Figure 1. *Lkb1*-deficient organoids display alterations in phenotype and reconstitution capacity.
A) Sequences of *Lkb1*-deficient organoids obtained with gRNA1 showing indels/deletions detected in exon 1 of the *Lkb1* gene. PAM sequences are underlined. **B)** Western blot of Lkb1 in WT and *Lkb1*-deficient organoids. **C)** Brightfield images of *Lkb1*-deficient organoid clones. Scale bar = 100 µM. **D)** Immunofluorescent images of cleaved caspase-3 (CC3, green) and F-actin (white) in *Lkb1*-deficient and WT organoids. Intraluminal (red arrowheads) and extraluminal $CC3^+$ cells (orange arrowheads) are indicated. Scale bar = 50 µm. **E)** Organoid reconstitution assay from single cells, cell viability was quantified at day 7. One-way ANOVA (Dunnett) was applied for analysis. * = $p < 0.05$. $N = 16$.

Figure 2. *Lkb1* loss mediates alterations in the number, location and ultrastructural morphology of secretory cells.
A) Immunofluorescence staining of Lysozyme1 (Lyz1, green) and F-actin (white) in WT and indicated *Lkb1*-deficient small intestinal organoids. Scale bar = 50 µm. White arrows indicate mislocalized $Lyz1^+$ cells. **B)** Immunohistochemistry staining of Mucin 2 (Muc2) in WT and indicated *Lkb1*-deficient organoids. Scale bar = 100 µm. **C-D)** Immunohistochemistry staining of MUC2 **(C)** and LYZ1 **(D)** in healthy and non-transformed PJS epithelium. Orange arrowheads indicate mislocalized $LYZ1^+$ cells. Scalebar upper panel = 500 µm, scalebar lower panel = 100 µm. **E-F)** Electron microscopy images Paneth **(E)** and goblet **(F)** cells in WT and indicated *Lkb1*-deficient organoids. Scale bar upper panel = 5 µm, lower panel = 1 µm.

Figure 3. *Lkb1* loss mediates increased expression of a regenerative gene signature in the intestinal epithelium.
A) GSEA of *Lkb1*-deficient versus WT organoids for cell types[33], colitis[35], injury[39], parasite[36], fetal spheroid[34], collagen[38] and revival stem cell[37] gene sets. Heatmap displays normalized enrichment scores (NES). ns = not significant, * = FDR < 0.05, ** = FDR ≤ 0.01, *** = FDR ≤ 0.001, **** = FDR ≤ 0.0001. **B)** Heatmap of z-score transformed expression values of $Lgr5^+$ stem cell genes (Stem)[33] enriched in WT organoids (top cluster) and fetal genes (Fetal)[34] enriched in *Lkb1*-deficient organoids (bottom cluster). Marker genes are highlighted. N = 3. **C)** Immunofluorescence staining of Anxa1 (green), DAPI (blue) and F-actin (red) in WT and *Lkb1*-deficient organoids. Fetal organoids from E16.5 mice are shown as a positive control. Scale bar = 50 µm**. D)** Immunohistochemistry staining of ANXA1 in healthy intestinal epithelium, PJS non-transformed epithelium and PJS dysplastic tissue. Scale bar upper panels = 250 µm, lower panels = 100 µm

Figure 4. *Lkb1*-deficiency accommodates Yap pathway activation and mediates upregulation of EGF family receptors and their ligands to drive niche independency.
A) GSEA of *Lkb1*-deficient versus WT organoids for Yap gene sets[40.42]. Heatmap displays normalized enrichment scores (NES). ns = not significant, * = FDR < 0.05, *** = FDR ≤ 0.001, **** = FDR ≤ 0.0001. **B)** Immunofluorescence staining for Yap (green), DAPI (blue) and F-actin (red) in WT and *Lkb1*-deficient organoids. Scale bar = 50 µm. **C)** Quantification of the nuclear fraction of Yap. $N = 13$ for WT organoids, $N = 19$ for $Lkb1^{+/-}$ organoids and $N = 17$ for $Lkb1^{bud\ -/-}$ organoids. One-way ANOVA was applied for analysis. **D-E)** Cumulative normalized counts of *Egfr* ligands **(D)** and *Egf* family receptors **(E)** in wild-type (WT) and

indicated *Lkb1*-deficient organoids. One-way ANOVA was applied for analysis. *N* = 3. **F)** Representative bright field images of WT and *Lkb1*-deficient organoids grown in the presence (ENR) and absence (NR) of Egf. Scale bar = 500 µm. **G)** Surface area covered by WT and *Lkb1*-deficient organoids grown in ENR or NR. *N* = 2-3. Two-way ANOVA was applied for analysis. **H)** Bright field images of WT and indicated *Lkb1*-deficient organoids cultured in NR and treated with DMSO or 100 nM Gefitinib. Scale bar = 500 µm. ** = p < 0.05, ** = p < 0.01 and **** = p < 0.0001.*

Figure 5. *Lkb1*-deficiency modifies intestinal stem cell identity.
A-B) UMAP of scRNA-seq data from WT Adult, WT fetal and *Lkb1*-deficient organoids. Colors indicate the different organoids lines **(A)** and the different cell types **(B)**. **C-D)** UMAP of scRNA-seq data from reclustered wild-type (WT (Adult)), *Lkb1*$^{+/-}$ and *Lkb1*$^{bud\ -/-}$ organoids. Colors indicate the different organoids lines **(C)** and the different cell types **(D)**. **E)** Percentage of cell types for each organoid line. **F)** Scatter plot showing module scores for Paneth[33] (y-axis) and goblet[33] (x-axis) cell signatures across all cells of wild-type (WT (Adult)), *Lkb1*$^{+/-}$ and *Lkb1*$^{bud\ -/-}$ organoids. Color indicates the origin of the cell. **G)** Expression of *Anxa1* onto the UMAP plot. **H)** GSEA on genes differentially expressed between WT and *Lkb1*-deficient stem cells for cell types[33], colitis[35], embryonic spheroid[34], collagen[38], Yap regeneration[40] and Yap overexpression[42] gene sets. Heatmap displays normalized enrichment scores (NES). ns = not significant, * = FDR < 0.05, *** = FDR ≤ 0.001, **** = FDR ≤ 0.0001. **I-J)** Violin plot showing module scores for goblet cell gene signature[33] **(I)** or *Anxa1* **(J)** across WT stem cells, *Lkb1*$^{+/-}$ stem cells and *Lkb1*$^{bud\ -/-}$ stem cells. ns = not significant, **** = p ≤ 0.0001 using one-way ANOVA with Wilcoxon test.

Figure 6. *Lkb1* loss drives a pre-malignant program along the serrated pathway that is further amplified by *Kras* mutations. A) GSEA of *Lkb1*-deficient versus WT organoids for serrated-specific[48], adenoma-specific[48], iCMS2[61] and iCMS3[61] genesets. Heatmap displays normalized enrichment scores (NES). ns = not significant, * = FDR < 0.05, *** = FDR ≤ 0.001, **** = FDR ≤ 0.0001. **B)** Heatmap of z-score transformed expression values of ASC[48] genes enriched in WT organoids (top cluster) and SSC[48] genes enriched in *Lkb1*-deficient organoids (bottom cluster). N = 3. **C-D)** Organoid reconstitution assay from single cells at day 7 for *Kras*-mutant and *Kras*-mutant/*Lkb1*-deficient organoids **(C)** or *Apc*-deficient and *Apc/Lkb1*-deficient organoids **(D)**. *N* = 8 **E-F)** Gene Set Variation Analysis (GSVA) analysis of SSC[48] genes **(E)** and ASC[48] genes **(F)** for WT, *Apc* mutant, *Kras* mutant, *Lkb1*-deficient, *Apc/Lkb1* double mutant and *Kras*/*Lkb1* double mutant organoids. *N* = 3. *O*ne-way ANOVA with Wilcoxon test was applied for analysis. **G)** Percentage of samples mutated for *BRAF, RNF43, PIK3CA, APC, KRAS* or *TP53* in *LKB1* WT (*N* = 7784) and *LKB1*-mutant (*N* = 83) colorectal tumors according to cBioPortal. Benjamini-Hochberg was applied for analysis. ** = FDR < 0.05, ** = FDR < 0.01 and **** = FDR < 0.0001.* **H)** Percentage of samples that are instable, stable, indeterminable, or not reported for microsatellite (MSI) status in *LKB1* WT (N = 2424) and *LKB1*-mutant (N = 28) colorectal tumors. **I-J)** Box plots showing log2 Z-scores for the *Lkb1*-deficient signature over the colon adenocarcinoma TCGA bulk RNA sequencing dataset grouped as mucinous (*N* = 68) or non-mucinous (*N* = 437) **(I)** or consensus molecular subtype (CMS1; *N* = 63, CMS2; *N* = 125, CMS3; *N* = 45, CMS 4; *N* = 73) **(J)** Welch's unequal variances t-test was applied for analysis. *ns = not significant, * = p < 0.05, ** = p < 0.01 and **** = p < 0.0001*.

Figure 1

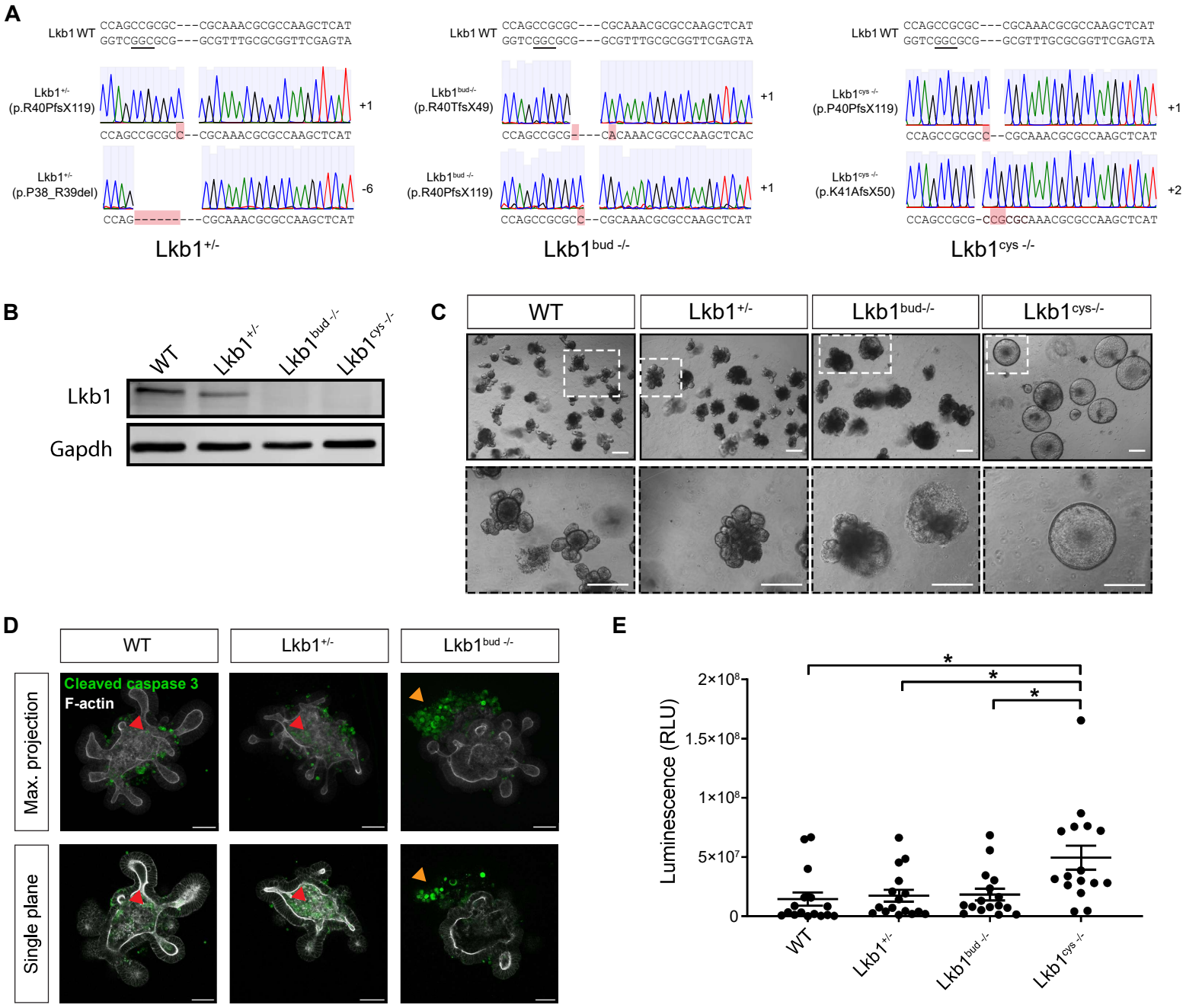
A
Lkb1 WT
CCAGCCGCGC---CGCAAACGCGCCAAGCTCAT
GGTCGGCGCG---GCGTTTGCGCGGTTCGAGTA
Lkb1+/- (p.R40PfsX119)
+1
CCAGCCGCGCC--CGCAAACGCGCCAAGCTCAT
Lkb1+/- (p.P38_R39del)
-6
CCAG-------CGCAAACGCGCCAAGCTCAT
Lkb1+/-
Lkb1bud-/- (p.R40TfsX49)
CCAGCCGCG---CACAAACGCGCCAAGCTCAC
Lkb1bud -/- (p.R40PfsX119)
Lkb1bud -/-
Lkb1cys -/- (p.P40PfsX119)
Lkb1cys -/- (p.K41AfsX50)
+2
CCAGCCGCG-CCGCGCAAACGCGCCAAGCTCAT
Lkb1cys -/-
B
WT
Lkb1+/-
Lkb1bud -/-
Lkb1cys -/-
Lkb1
Gapdh
C
WT
Lkb1+/-
Lkb1bud-/-
Lkb1cys-/-
D
WT
Lkb1+/-
Lkb1bud -/-
Max. projection
Single plane
Cleaved caspase 3
F-actin
E
Luminescence (RLU)
2×10^8
1.5×10^8
1×10^8
5×10^7
0
*
*
*
WT
Lkb1+/-
Lkb1bud -/-
Lkb1cys -/-

Figure 2

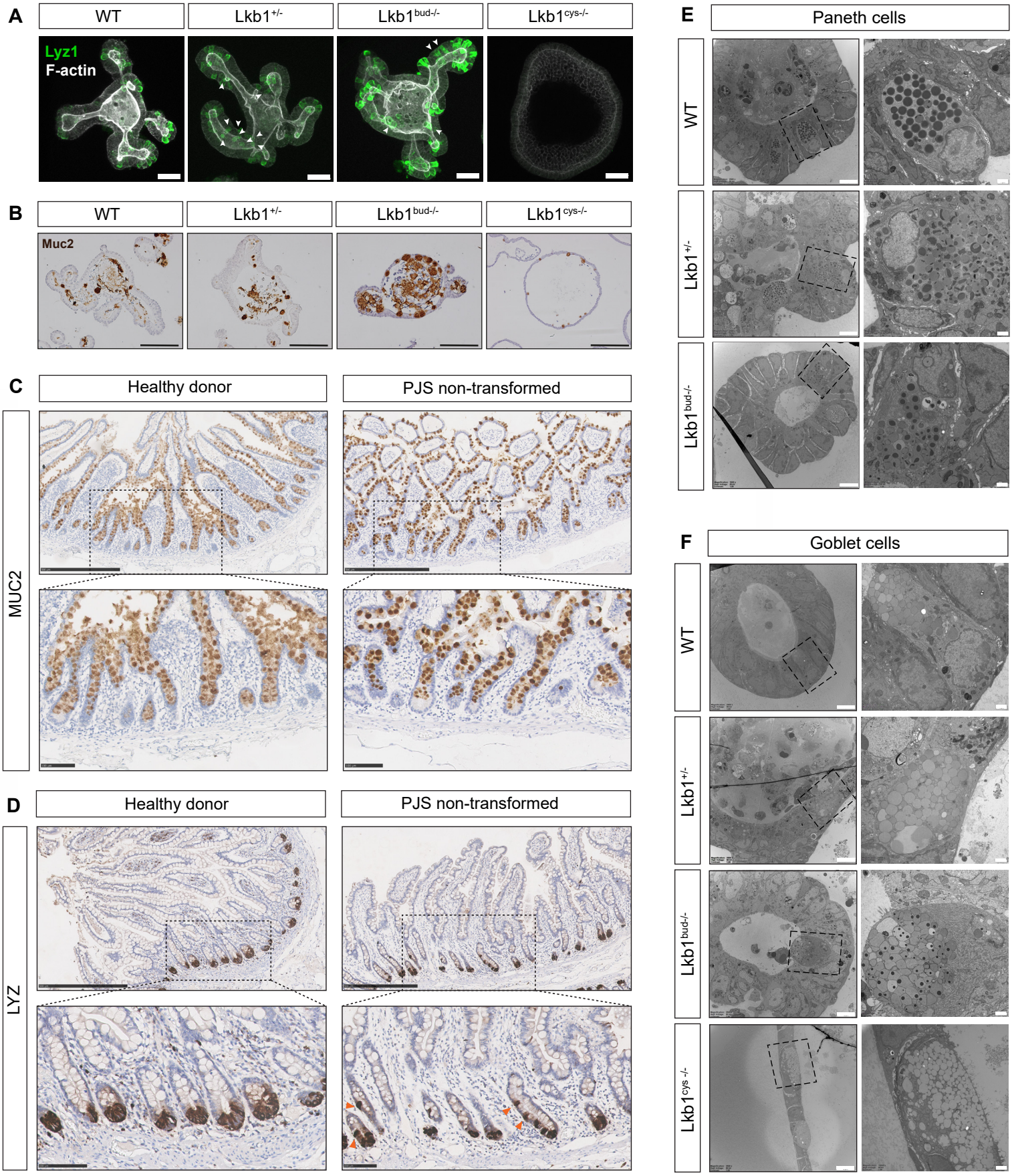
A
WT
Lkb1+/-
Lkb1bud-/-
Lkb1cys-/-
Lyz1
F-actin
B
WT
Lkb1+/-
Lkb1bud-/-
Lkb1cys-/-
Muc2
C
Healthy donor
PJS non-transformed
MUC2
D
Healthy donor
PJS non-transformed
LYZ
E
Paneth cells
WT
Lkb1+/-
Lkb1bud-/-
F
Goblet cells
WT
Lkb1+/-
Lkb1bud-/-
Lkb1cys -/-

Figure 3

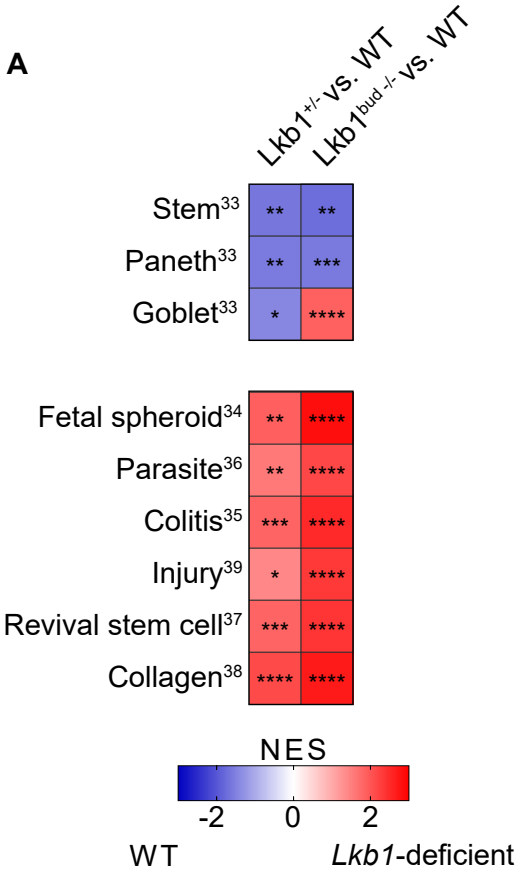
A
Lkb1+/- vs. WT
Lkb1bud -/- vs. WT
Stem33
Paneth33
Goblet33
Fetal spheroid34
Parasite36
Colitis35
Injury39
Revival stem cell37
Collagen38
NES
-2
0
2
WT
Lkb1-deficient

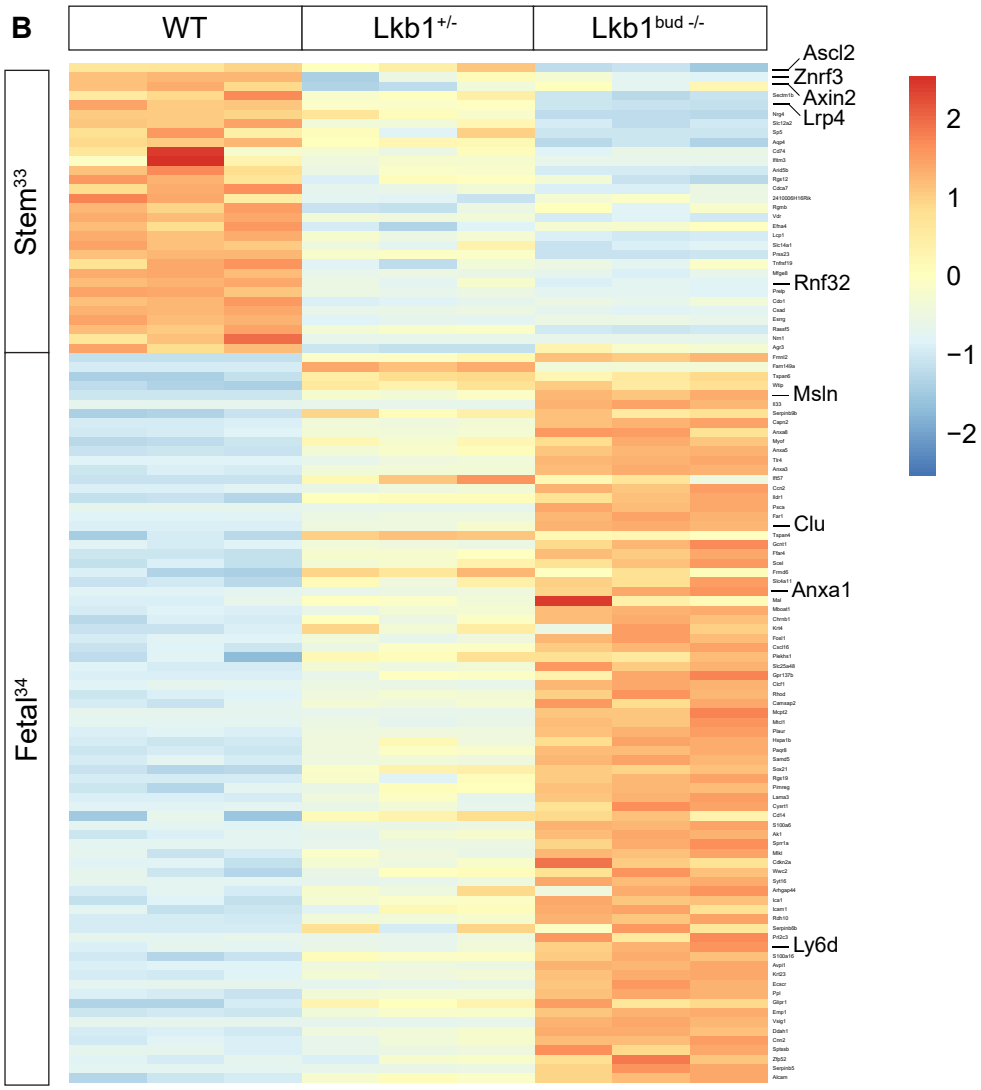
B
WT
Lkb1+/-
Lkb1bud -/-
Stem33
Fetal34
Ascl2
Znrf3
Axin2
Lrp4
Rnf32
Msln
Clu
Anxa1
Ly6d
2
1
0
−1
−2

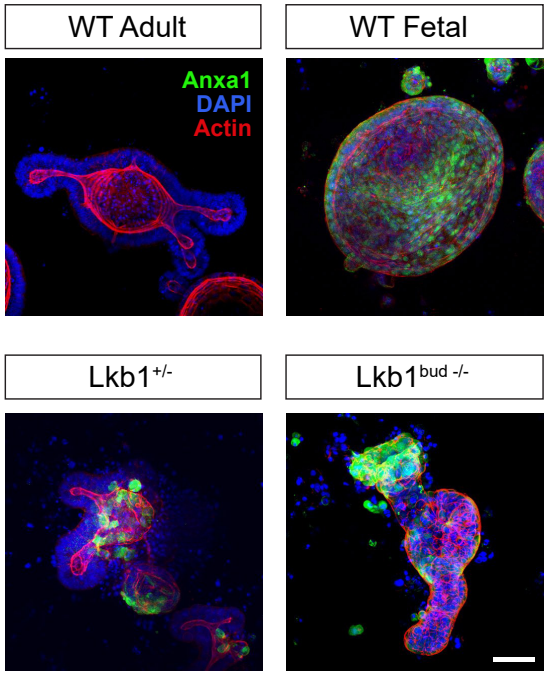
C
WT Adult
WT Fetal
Anxa1
DAPI
Actin
Lkb1+/-
Lkb1bud -/-

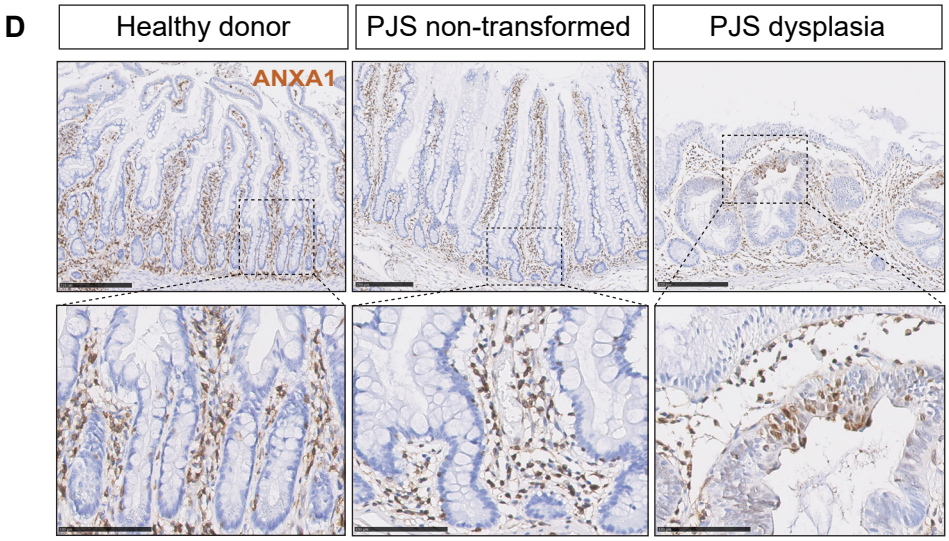
D
Healthy donor
PJS non-transformed
PJS dysplasia
ANXA1

Figure 4

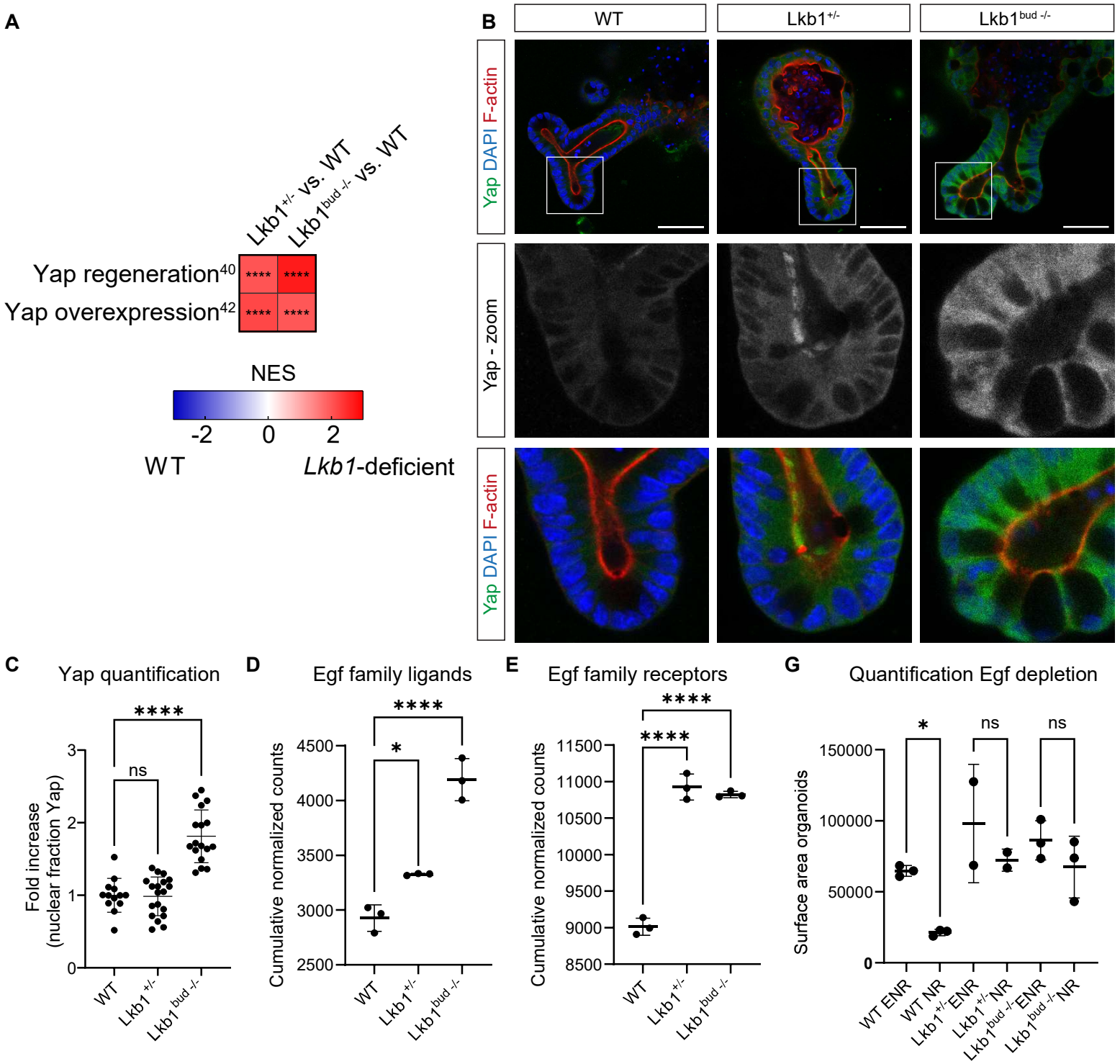
A
Lkb1+/- vs. WT
Lkb1bud -/- vs. WT
Yap regeneration40
Yap overexpression42
****
NES
-2
0
2
WT
Lkb1-deficient
B
WT
Lkb1+/-
Lkb1bud -/-
Yap DAPI F-actin
Yap - zoom
C
Yap quantification
Fold increase (nuclear fraction Yap)
ns
D
Egf family ligands
Cumulative normalized counts
*
E
Egf family receptors
G
Quantification Egf depletion
Surface area organoids
ns
WT ENR
WT NR
Lkb1+/-ENR
Lkb1+/-NR
Lkb1bud -/-ENR
Lkb1bud -/-NR

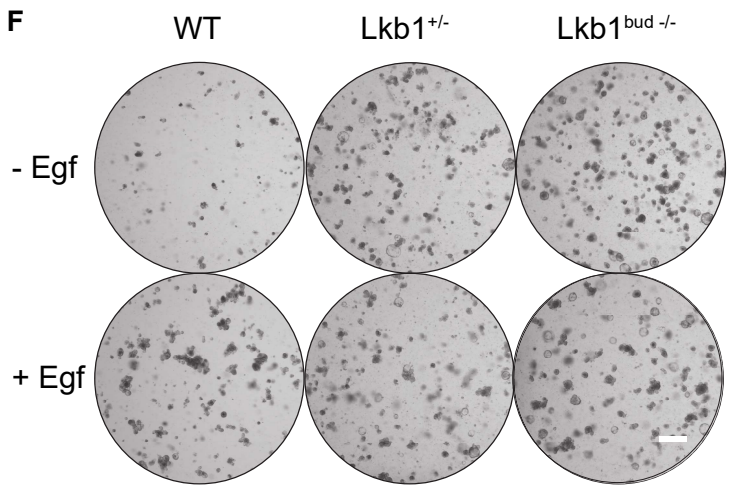
F
WT
Lkb1+/-
Lkb1bud -/-
- Egf
+ Egf

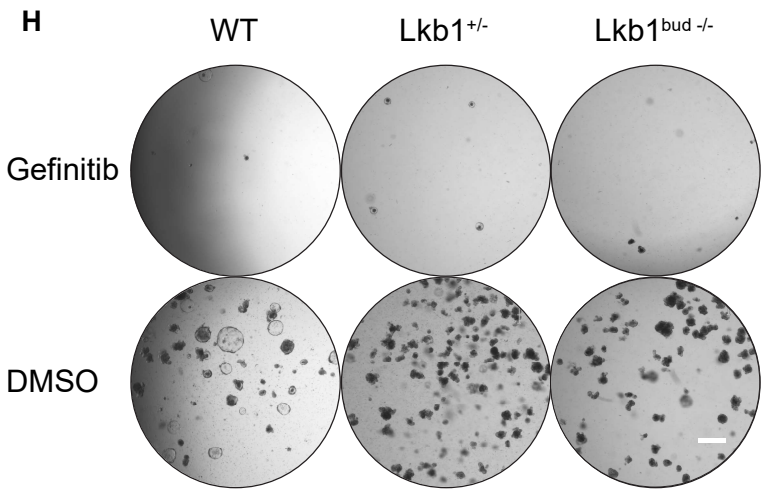
H
WT
Lkb1+/-
Lkb1bud -/-
Gefinitib
DMSO

Figure 5

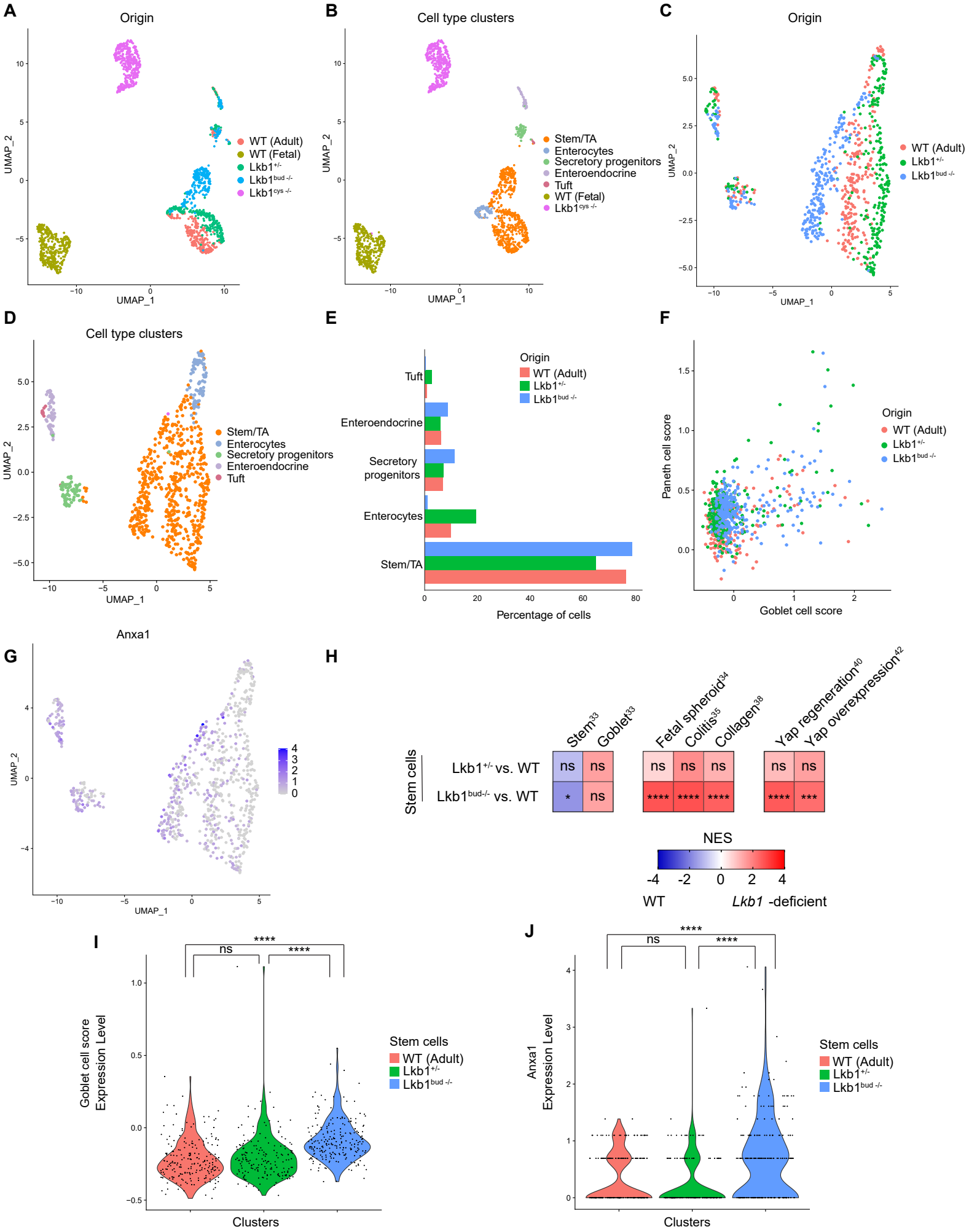
A
Origin
UMAP_1
UMAP_2
WT (Adult)
WT (Fetal)
Lkb1+/-
Lkb1bud -/-
Lkb1cys -/-
B
Cell type clusters
Stem/TA
Enterocytes
Secretory progenitors
Enteroendocrine
Tuft
WT (Fetal)
Lkb1cys -/-
C
Origin
WT (Adult)
Lkb1+/-
Lkb1bud -/-
D
Cell type clusters
Stem/TA
Enterocytes
Secretory progenitors
Enteroendocrine
Tuft
E
Origin
WT (Adult)
Lkb1+/-
Lkb1bud -/-
Tuft
Enteroendocrine
Secretory progenitors
Enterocytes
Stem/TA
Percentage of cells
F
Paneth cell score
Goblet cell score
Origin
WT (Adult)
Lkb1+/-
Lkb1bud -/-
G
Anxa1
H
Stem cells
Lkb1+/- vs. WT
Lkb1bud-/- vs. WT
Stem33
Goblet33
Fetal spheroid34
Colitis35
Collagen38
Yap regeneration40
Yap overexpression42
ns
*
****
***
NES
WT
Lkb1 -deficient
I
Goblet cell score Expression Level
Clusters
Stem cells
WT (Adult)
Lkb1+/-
Lkb1bud -/-
J
Anxa1 Expression Level
Clusters
Stem cells
WT (Adult)
Lkb1+/-
Lkb1bud -/-

Figure 6

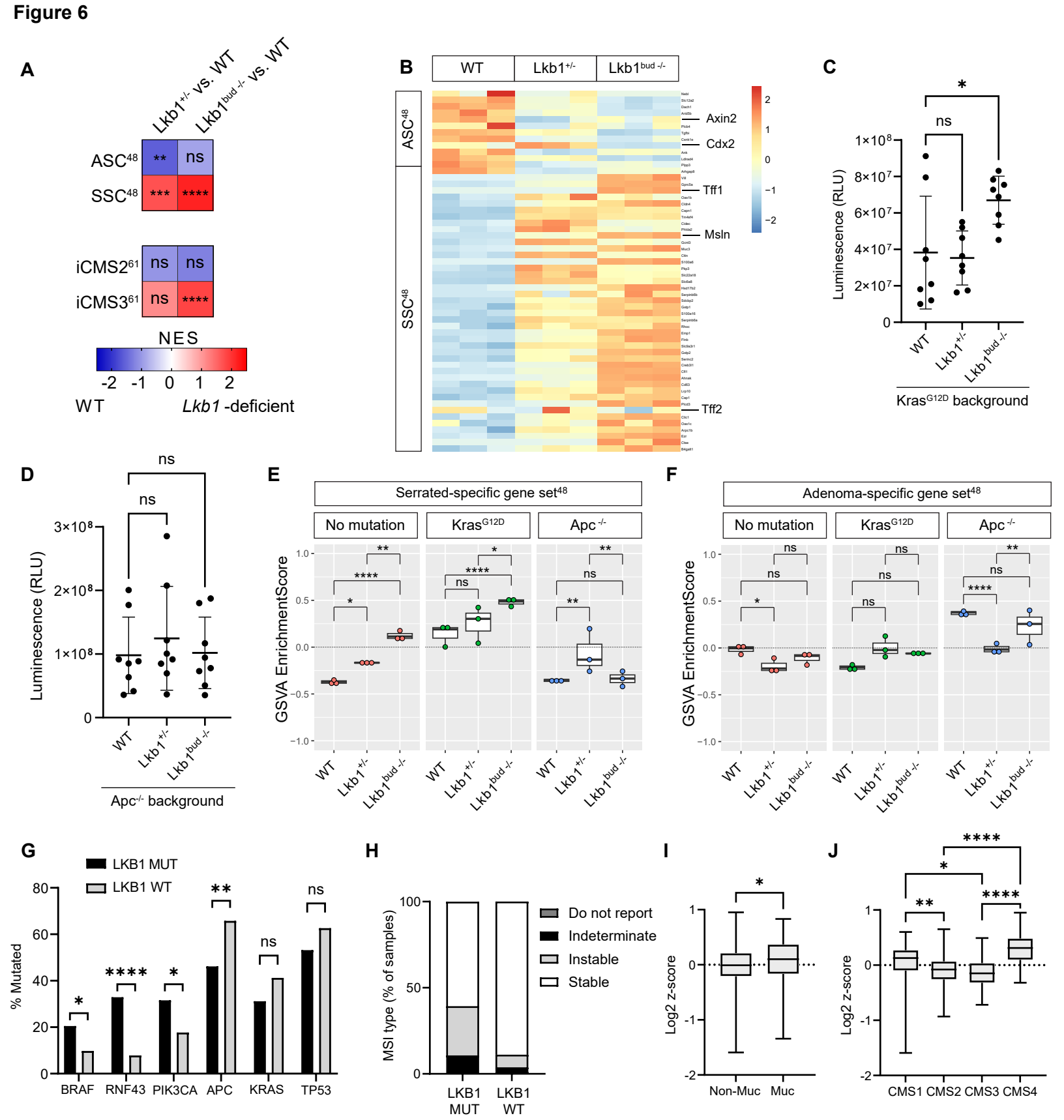
A
Lkb1+/- vs. WT
Lkb1bud -/- vs. WT
ASC48
SSC48
iCMS261
iCMS361
NES
WT
Lkb1 -deficient
B
WT
Lkb1+/-
Lkb1bud -/-
ASC48
SSC48
Axin2
Cdx2
Tff1
Msln
Tff2
C
Luminescence (RLU)
KrasG12D background
D
Luminescence (RLU)
Apc-/- background
E
Serrated-specific gene set48
No mutation
KrasG12D
Apc -/-
GSVA EnrichmentScore
F
Adenoma-specific gene set48
No mutation
KrasG12D
Apc -/-
GSVA EnrichmentScore
G
LKB1 MUT
LKB1 WT
% Mutated
BRAF
RNF43
PIK3CA
APC
KRAS
TP53
H
MSI type (% of samples)
Do not report
Indeterminate
Instable
Stable
LKB1 MUT
LKB1 WT
I
Log2 z-score
Non-Muc
Muc
J
Log2 z-score
CMS1
CMS2
CMS3
CMS4